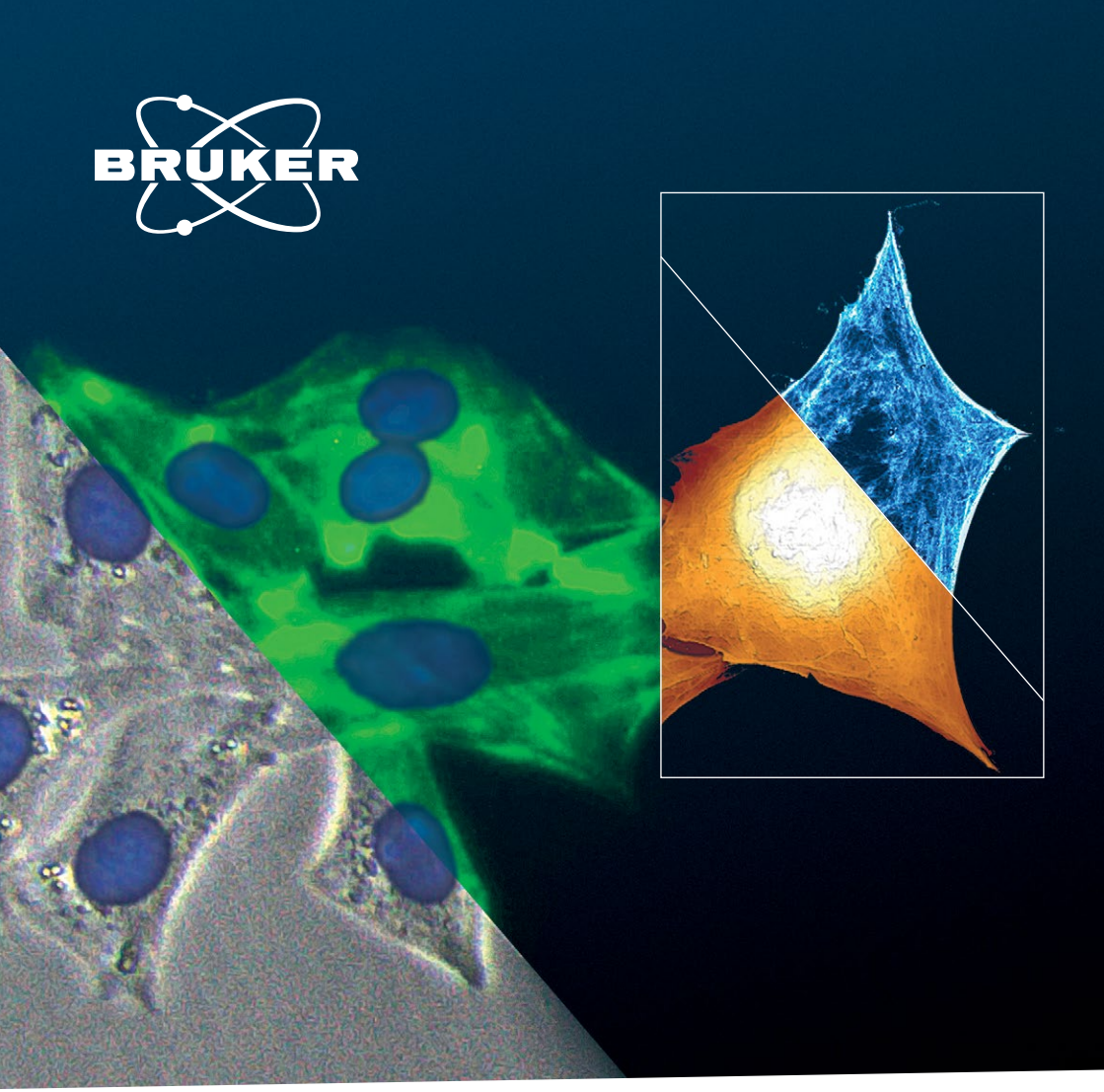

ATOMIC FORCE MICROSCOPY

Correlative AFM and Optical Microscopy in Life Science Research

A Brief Overview

Table of Contents

Introduction

The intricate details of small objects, invisible to the human eye, have always fascinated humankind. Historically, understanding biological complexity relied on the principle of "seeing is believing". Recent decades have seen substantial advancements in the field of microscopy, driven by the desire to unravel the relationship between structure and function in cells, organelles, and biomolecules.

Conventional light microscopy provides an enlarged, two-dimensional view of a sample by illuminating it with visible light and viewing it through an optical lens system. However, the resolution is limited by the wavelength of the light used, known as the Abbe diffraction limit, whereby only objects larger than approx. 250 nm can be sharply imaged.[1] In 1986, atomic force microscopy (AFM) emerged as a new three-dimensional approach,[2] quickly becoming a standard for the high-resolution structural analysis of samples ranging from single molecules to complex macromolecular systems.

AFM uses a sharp tip to scan the surface of an object, generating three-dimensional topographical images with nanometer resolution. In addition, it enables the multiparametric, quantitative characterization of a sample's nanomechanical properties. AFM can be combined with other microscopy techniques, such as optical microscopy, to reveal additional aspects of a sample, providing multi-level analysis and a more comprehensive understanding of the sample.

By combining AFM with fluorescent microscopy, specific molecules or features carrying immunochemical information can be directly targeted.[3] Both AFM and light microscopy can be operated under ambient environmental conditions, enabling live-cell imaging and leveraging the advantages of both techniques. The ability to obtain real-time, correlative data sets is particularly relevant in life science research.

Novel super-resolution microscopy approaches have emerged in light microscopy that surpass the diffraction limit of light,[4] such as structured illumination microscopy (SIM),[5] single-molecule localization microscopy (SMLM),[6,7] and stimulated emission depletion microscopy (STED).[8] Combining AFM with these advanced optical techniques is a powerful approach for investigating biological samples at the nanoscale that delivers profound new insights into molecular and cellular mechanisms and the relationship between structure and function.

Correlative Microscopy – The Basics

While an AFM can operate as a stand-alone system, providing excellent resolution and direct access to the sample, it is often paired with basic optical systems. This combination provides a larger field of view and facilitates navigation to specific areas of interest on the sample, as the scan size of the AFM is typically limited to around 100 µm × 100 µm. Additionally, the combination of AFM with an optical system simplifies the alignment of the cantilever detection system. By integrating AFM with optical techniques, such as fluorescence microscopy, it is also possible to characterize the biochemical composition of a sample.

Optical microscopes are generally categorized into two types: upright and inverted setups.

Combining AFM with Upright Optical Microscopy

In upright microscopes, the objective lenses are positioned above the sample, enabling the examination of both opaque and transparent samples. When AFM is integrated with these optical systems, both must operate from the same side of the sample (see Figure 1). However, this configuration limits optical resolution because high-resolution optics require objectives with very short working distances, leaving insufficient space for the AFM probe to access the sample.

To overcome this limitation, Bruker has developed a specialized solution known as the BioMaterials Workstation (BioMAT). This system consists of a shuttle stage that securely holds the sample and can be transferred between the AFM and a high-resolution upright optical microscope with high positioning accuracy. This setup allows sequential examination of the same sample area with both the AFM and high-resolution upright optics. This solution is ideal for the correlated study of samples on non-transparent substrates, such as tissue sections, bacterial growth on metallic surfaces, and biochips.

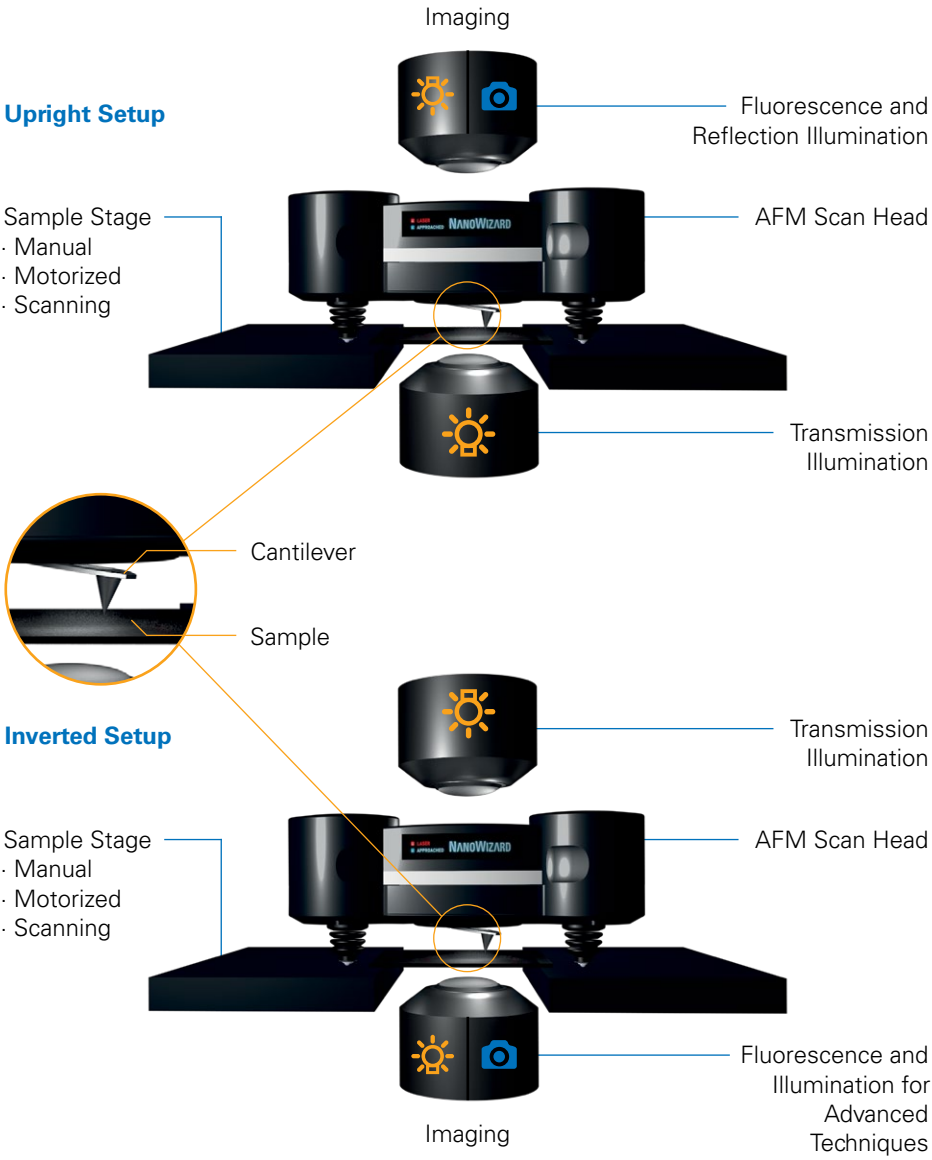

Figure 1

Scheme for the integration of the NanoWizard® AFM platform into various types of optical microscopes. The scan head of the AFM is positioned above the stationary sample and can scan along all three axes (X, Y and Z). The region around the central axis of the AFM head is optically transparent, enabling access for illumination or imaging from above.

Recently, there has been a growing demand for AFM systems that can be integrated with upright fluorescence microscopes for the characterization of larger samples, such as thick tissue slices, implants, and biomaterials. For such samples, where high optical resolution is less critical, AFM can be paired with upright zoom microscopes like the Zeiss AxioZoom.V16 (see Figure 2). These microscopes feature long working distance objectives, providing ample space for the AFM to access the sample.

Combining AFM with Inverted Optical Microscopy

In inverted optical microscopes, the objective is located beneath the sample. These microscopes are primarily designed for transparent samples, with the illumination typically coming from above. Most conventional and advanced optical microscopy solutions are commonly based on inverted optical microscopes. Offering high-resolution optical imaging and great flexibility, they have become the de facto standard in life science research. Inverted microscopes are particularly well suited for integration with AFM, as the optics and AFM can operate on opposite sides of the sample without interfering with each other, unlike in upright microscopy.

As most advanced optical techniques are based on inverted optical microscope platforms, they can be easily combined with AFM. This includes techniques like STED, photo-activated localization microscopy and stochastic optical reconstruction microscopy (PALM/STORM), total internal reflection fluorescence microscopy (TIRFM), Förster resonance energy transfer (FRET), fluorescence lifetime imaging microscopy (FLIM), and more. Many of these techniques use fluorescence, which is particularly useful when combined with AFM, as fluorescence labeling complements the capabilities of AFM by identifying specific biomolecules, chemicals, cell structures, organelles or antigens.

Bruker's NanoWizard AFM heads have been specifically designed to allow their seamless integration with optics (see figure 1) and to be combined with all major brands of optical microscopes. All NanoWizard models feature a tip-scanning design that allows the

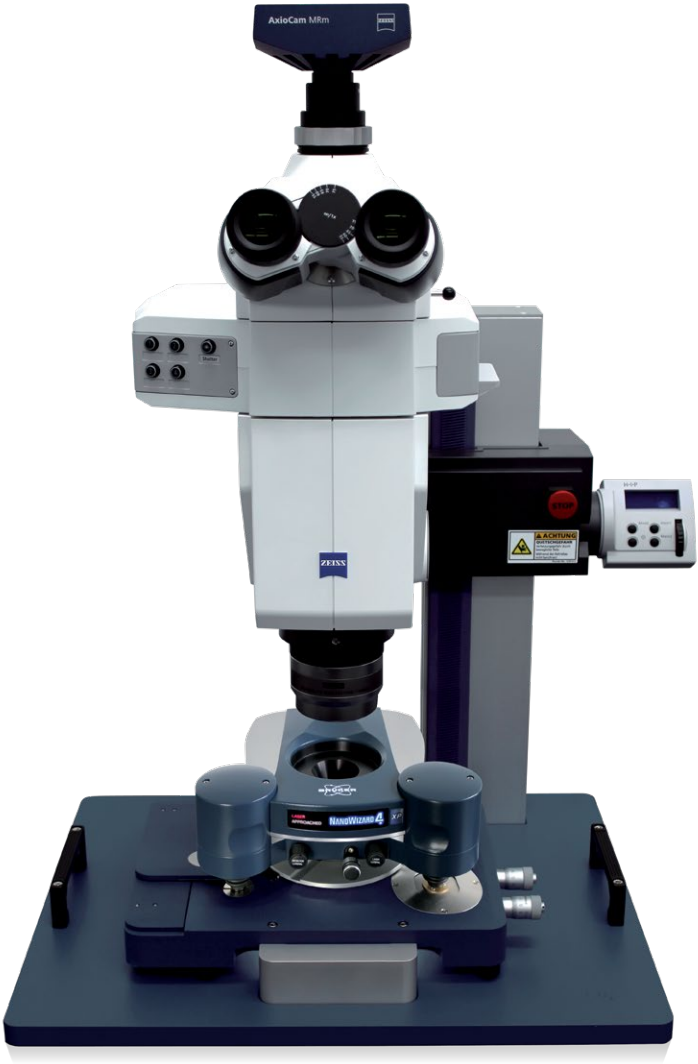

Figure 2

The integration of a NanoWizard 4XP AFM system (Bruker) with an Axio Zoom.V16 upright fluorescence microscope (Zeiss) enables the investigation of large sample areas on opaque samples.

AFM probe to scan in all three directions (X, Y, and Z) while the sample remains stationary. This is beneficial in applications where the optical image of the sample should not move during the AFM measurements, facilitating the simultaneous, time-lapse collection of both AFM and optical data.[9] Furthermore, tip-scanning systems can accommodate larger and heavier samples and are easier to integrate with advanced optical techniques than sample scanning systems.

Despite the numerous advantages of tip-scanning AFM, certain optical techniques require the sample to move instead, in particular when the AFM tip is used as an active element in the optical setup and must be stationary relative to the optical focal point. Such techniques include tip-enhanced Raman spectroscopy (TERS),[10] scanning near-field optical microscopy (SNOM),[11] tip-assisted FLIM,[12-14] and FRET. To integrate the NanoWizard series AFMs with these optical techniques, Bruker offers the Tip-Assisted-Optics (TAO) module, a stage that scans the sample while the tip scanner can be used for fine tuning and alignment of the AFM tip position relative to the optical path.

General Considerations on Integrating AFM with Optical Microscopy

While AFM scanning is highly precise, standard optical microscopes are subject to non-linearities, making it almost impossible to accurately correlate AFM scans with optical images based on linear scaling alone. To address this issue, Bruker developed the DirectOverlay software feature, a patented solution that allows the precise integration of AFM with optical microscopy. It achieves accurate correlation by performing a non-linear correction of the optical images based on a calibration process that uses the precise movement of the AFM scanner. This calibration only needs to be performed once for an objective as it can be conveniently saved and reused.

When performing correlated AFM measurements on large samples like tissues, optical mircoscopes are often not capable of providing an overview of the entire sample.

Bruker's DirectTiling software module addresses this by automatically stitching together multiple high-resolution optical images to form a comprehensive overview. This process requires a motorized sample stage that allows the sample to be moved over a large area.

DirectTiling integrates seamlessly with the DirectOverlay feature, allowing precise navigation on the sample and the selection of multiple measurement positions within the acquired overview image, either manually or via AI features. Using Bruker's MultiScan or SmartMapping feature, the pre-selected areas of interest can be examined fully automatically with the AFM. This makes DirectTiling indispensable for optically guided AFM experiments that demand highly precise scanning of large sample areas.

When integrating AFM with advanced optical microscopy, there are some important aspects to consider. Vibrations from the optical system, such as those caused by fans or other moving parts, can be transmitted to the AFM measurement, affecting its accuracy or quality. This is especially critical when using high-resolution optical techniques like STED and confocal microscopy that require thin glass substrates and immersion media in order to use lenses with a high numerical aperture. However, these thin substrates are particularly susceptible to vibrations, and the viscous immersion medium can also transfer vibrations from the microscope directly to the sample. To address these issues, specialized liquid cells such as the CoverslipHolder and BioCell (Bruker) can be used to stabilize AFM measurements on thin glass coverslips.

When integrating with certain optical systems, simultaneous optical and AFM imaging may not always be feasible. This is particularly true for optical methods that use a powerful laser, which can cause the AFM probe to bend due to thermal effects or photopressure, thus interfering with AFM imaging. Conversely, the AFM detection laser can also disrupt the optical measurement. In such cases, optical and AFM measurements must be performed sequentially. Bruker offers extensive routines for automating such processes.

Case Studies

The following section outlines several innovative experiments that highlight the potential of correlative microscopy for advancing our understanding of complex biological mechanisms at the nanoscale level.

Studying the Role of Tissue Mechanics in Neurogenesis and Brain Damage using Fluorescence-Guided Navigation

There is an increasing awareness of the integral role tissue mechanics play in disease progression and organogenesis. Microscopic investigation of tissue samples often requires the examination of large sample regions, spanning several hundred micrometers to millimeters.

Neurons are particularly sensitive to their mechanical environment. The stiffness of the surrounding tissues serves as a guidance cue during neurogenesis. In the developing brains of Xenopus, neurons of the optic tract extend axons into the brain to connect to the optic center. At a specific location, these neurons must change direction to stay on course. Previous studies have measured the local stiffness of the brain tissue at this turning point, demonstrating that the local change in stiffness indeed serves as a guidance cue for axonal turning.[15]

In the dentate gyrus of the hippocampus, new neurons are continuously generated, even in adult mice. From there, these neurons subsequently migrate to their final positions. Newly formed neurons express GFP-labeled nestin, which ceases to be expressed as the neurons age, thus serving as a useful marker. Using DirectOverlay, it was possible to precisely align fluorescent images with AFM maps of the local tissue stiffness (see Figure 3). This revealed that the region where neurons are formed is softer than the surrounding areas.

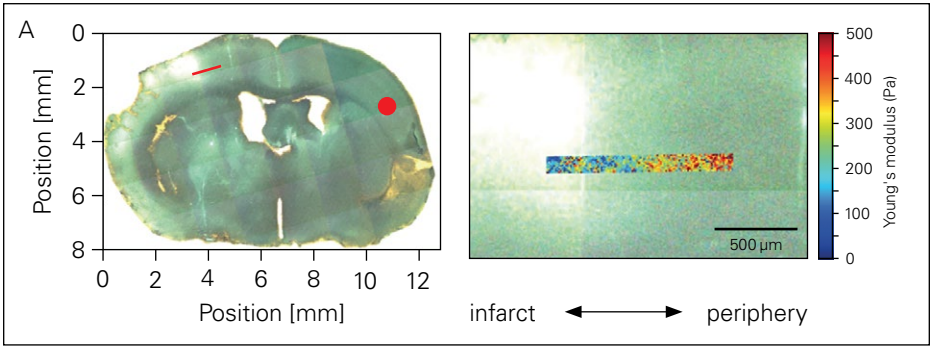

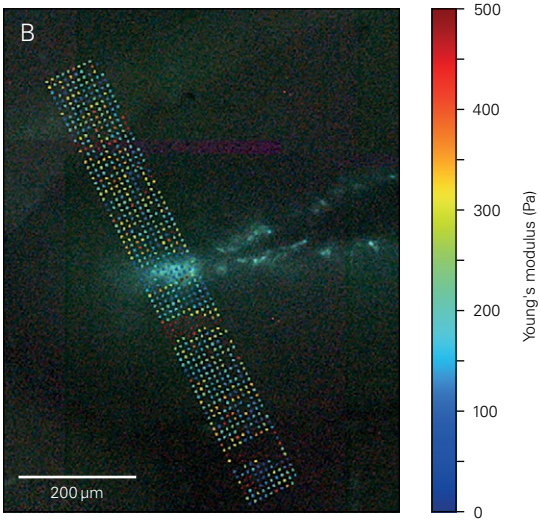

Figure 3

AFM analysis and fluorescent imaging of brain slices.

(A) Mouse brain slice area affected by ischemic stroke. The bright regions represent FITC-albumin labels, indicating albumin diffusion from damaged blood vessels into the brain tissue affected by ischemic stroke. A stiffness map (100 µm × 1100 µm) was generated across the edge of the infarcted region. Optical images were captured using Zeiss Axio Zoom.V16.

(B) Force mapping across the dentate gyrus of a mouse hippocampus. Newly formed neurons are marked by the expression of GFP-labeled nestin. The DirectOverlay feature enables precise registration of the AFM map and the fluorescent image, thus facilitating the correlation of the fluorescent signal and tissue stiffness.

Figures (A) and (B) were adapted from[17] and[16] respectively, under the open access usage policy.

By performing a force map over an area of several hundred micrometers, *in vitro* high-resolution elasticity data from AFM was correlated with *in vivo* elasticity data collected with magnetic resonance elastography.[16]

To characterize the changes in Young's modulus in regions affected by ischemic stroke in mouse brains,[17] it was crucial to identify the boundary of the damaged area. This was performed using a fluorescent marker and the DirectTiling feature. When working with fresh, unfixed tissue, the measurement time is a critical factor that must be taken into consideration in order to avoid artifacts and changes to the Young's modulus. Given that a whole brain slice is several millimeters in size, mapping the entire slice would be prohibitively time-consuming. In such cases, DirectOverlay is instrumental for the rapid identification of the region of interest, enabling the investigator to focus on relevant areas and minimize the duration of the measurement.

Visualizing the Cell Cycles of HeLa Cells with Correlative AFM-FLIM

AFM-FLIM – The Technique

Fluorescence lifetime imaging microscopy (FLIM) is a technique typically implemented as a variation of confocal microscopy. The operating principle is based on the differences in the exponential decay rates of fluorophores within a sample. In FLIM, the fluorescence lifetime of the fluorophore is used to generate additional contrast or extract functional information from images, in addition to the fluorescence intensity (see Figure 4). Although the concept of picosecond time-resolved fluorescence measurements dates back to the 1950s, FLIM emerged as a technique for mapping fluorescence lifetimes in 1989[18] and was further developed in the early 1990s.[19-21] FLIM provides fluorescence information in scenarios where intensity-based detection is challenging, such as in auto-fluorescent samples or FRET studies. Moreover, FLIM can provide additional insights into the local environment within the sample through fluorescent sensors.

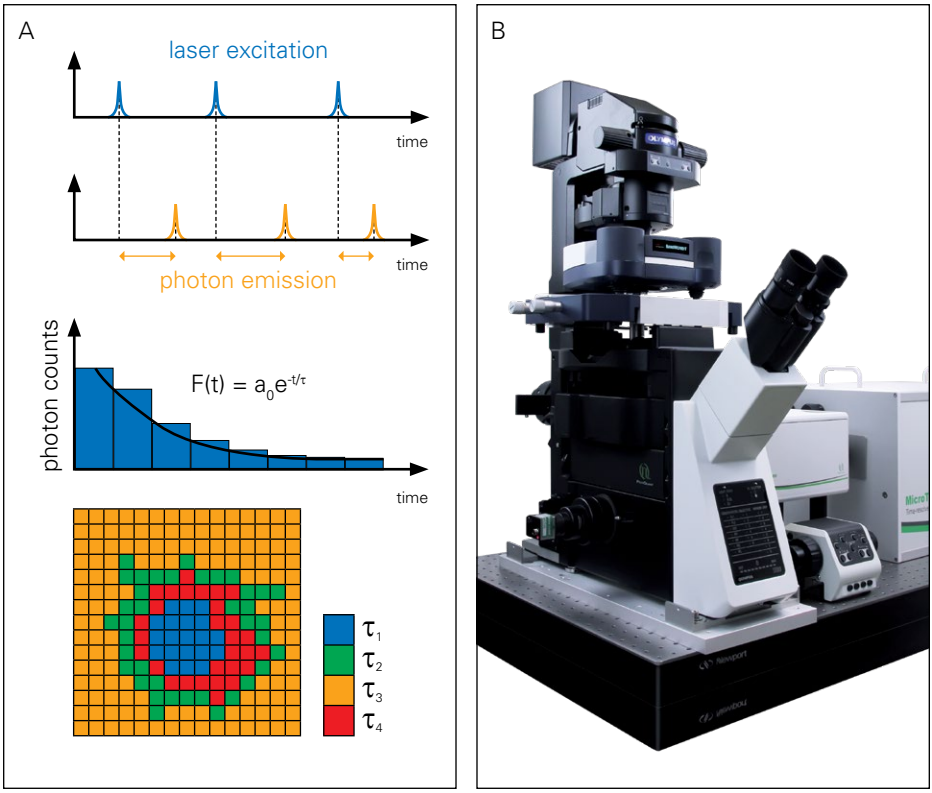

Figure 4

(A) Principle of FLIM data acquisition. The sample fluorescence is excited repeatedly by picosecond laser pulses (at a MHz rate) and the arrival time of the emitted photons, relative to the excitation pulse, is measured (time-tagging). A fluorescence lifetime τ image is generated by scanning the excitation laser in a line-wise manner across the sample. All photons for a given image pixel are grouped into a decay histogram, which is used to measure its fluorescence intensity (total photon count) and lifetime. The fluorescence lifetime is typically characterized by fitting a multi-exponential decay curve to the histogram of photon counts (amplitude, a_0) vs. post-laser pulse arrival time t. A basic fluorescence lifetime image example utilizes a color look-up table to display the different lifetime values (τ_1,τ_2, etc.).

(B) Combined setup of MicroTime 200 Confocal FLIM system (PicoQuant) and NanoWizard AFM (Bruker). The AFM sample stage (TAO module, 3-axis) is mounted onto the IX73 body (Olympus) of the MicroTime 200.

This can include information on parameters such as pH, viscosity, membrane tension, or chemical species concentration.

In correlative AFM, both the AFM and the optical technique are typically employed to observe the same region, potentially simultaneously. It's important to note that there is no intended interaction between the AFM cantilever tip and the optical illumination system. An integrated setup that combines AFM and optical FLIM can be specifically designed to exploit this interaction to locally modulate the fluorescence lifetime of the sample with nanometer precision. This is achieved by focusing the excitation laser of the FLIM at the tip of the cantilever. The TAO module adds an additional sample scanning stage that enables the cantilever to maintain perfect alignment in the laser focus while the sample is being imaged with the sample scanner.

AFM-FLIM can further increase the resolution as the fluorescent lifetime is only modulated in a nanometer-sized volume at the very tip of the AFM cantilever. To validate the exact positional congruence between both techniques in the AFM-FLIM setup described above, combined AFM-FLIM measurements were conducted with 200 nm fluorescent beads on a 170 µm thick glass coverslip. Figures 5A-C show the topography, fluorescence intensity, and fluorescence lifetime (FLIM) images, respectively, which were recorded simultaneously at the same XY-position.

To improve the signal-to-noise ratio in the optical image, an AFM-FLIM image (Figure 5D) with lower pixel resolution was then recorded. In the AFM images, the bead is represented by its accurate dimensions. However, the bead edge with a 200 nm diameter is clearly resolved as a ring of shortened fluorescence lifetime in Figure 5D with a much higher accuracy. The metal-coated AFM cantilever tip in contact with the bead's fluorophores decreases the fluorescence lifetime, whereas the pyramid shape of the cantilever (Multi75E-G, MikroMasch) creates different effective contact areas between the tip and the bead, reaching a maximum at the edge of the bead, and effectively causing the observed contrast.

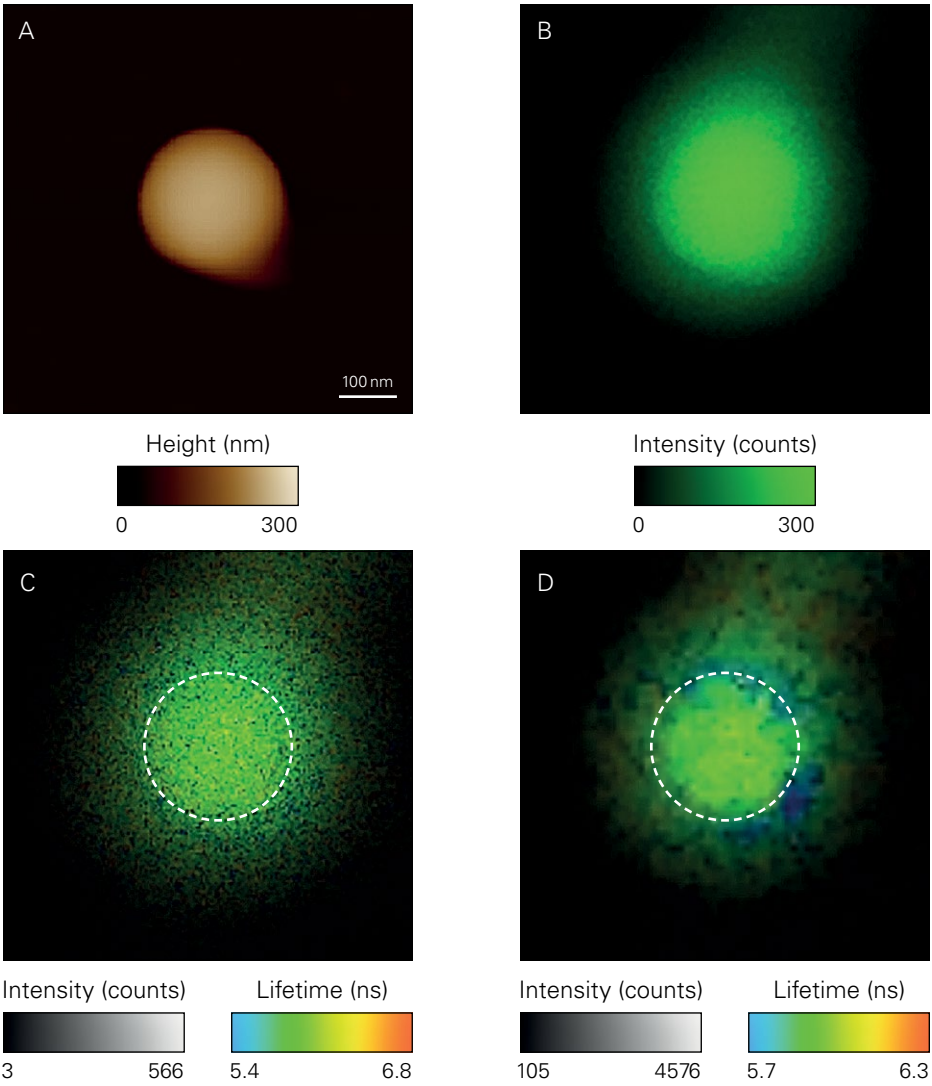

Figure 5

Combined AFM-FLIM measurement with a TAO stage.

(A) AFM topography, (B) fluorescence intensity and (C) fluorescence lifetime image of a single fluorescent bead (Molecular Probes, d = 200 nm). The bead's position, taken from the AFM topography, is marked in the corresponding fluorescence images (dashed circle). (D) Reconstructed fluorescence lifetime image using a lower pixel resolution to achieve a better signal to noise ratio. The fluorescence lifetime is significantly shortened at the bead edge.

The integration of AFM and FLIM with a TAO stage offers significant advantages for single-molecule measurements at the nanometer scale when AFM and fluorescence lifetime data need to be recorded simultaneously at the same position. However, for larger specimens, such as cells or tissues, it is often more practical to employ larger scale offsetting positional stages (discussed below), which allow areas of up to several centimeters to be surveyed. In such scenarios, AFM and FLIM data are typically recorded in a sequential manner, while focusing on the same region of interest.

Visualizing the Cell Cycle of HeLa Cells Using AFM-FLIM

Figure 6 illustrates correlative AFM-FLIM measurements performed using a Motorized Precision Stage on rehydrated HeLa cells in a buffer solution. The combined application of AFM and FLIM is pivotal for determining the stage of the cell cycle. While AFM provides superior resolution and is essential for characterizing the surface and mechanical properties of the cells, the combination with FLIM enables the identification of the distribution of microtubules and chromatin within the cells. For this purpose, the cells were engineered to express tubulin-EGFP, which fluorescently labels microtubules, and H2B-mCherry, which labels histones that compact DNA in the chromatin, primarily located in the nucleus.

A cluster of 23 cells was first identified via optical phase contrast and imaged by AFM as multiple tiles covering an area of 250 µm × 250 µm (Figure 6A), followed by a two-color FLIM recording in the highlighted location. The corresponding fluorescence lifetime images of EGFP (Figure 6B) and mCherry (Figure 6C) show the expected distribution of microtubules and chromatin within the cells. Notably, the clear chromatin separation in Figure 6C indicates a cell (outlined) residing in the metaphase of its cell division cycle. The fluorescence lifetime is encoded in the rainbow color scale, while fluorescence intensity is represented by brightness. The significant fluorescent background with a longer fluorescence lifetime observed for mCherry also indicates the presence of histones in the cell cytoplasm. Histones are typically synthesized by free ribosomes in the cytoplasm and are, therefore, not exclusively confined to the chromatin within the nucleus.

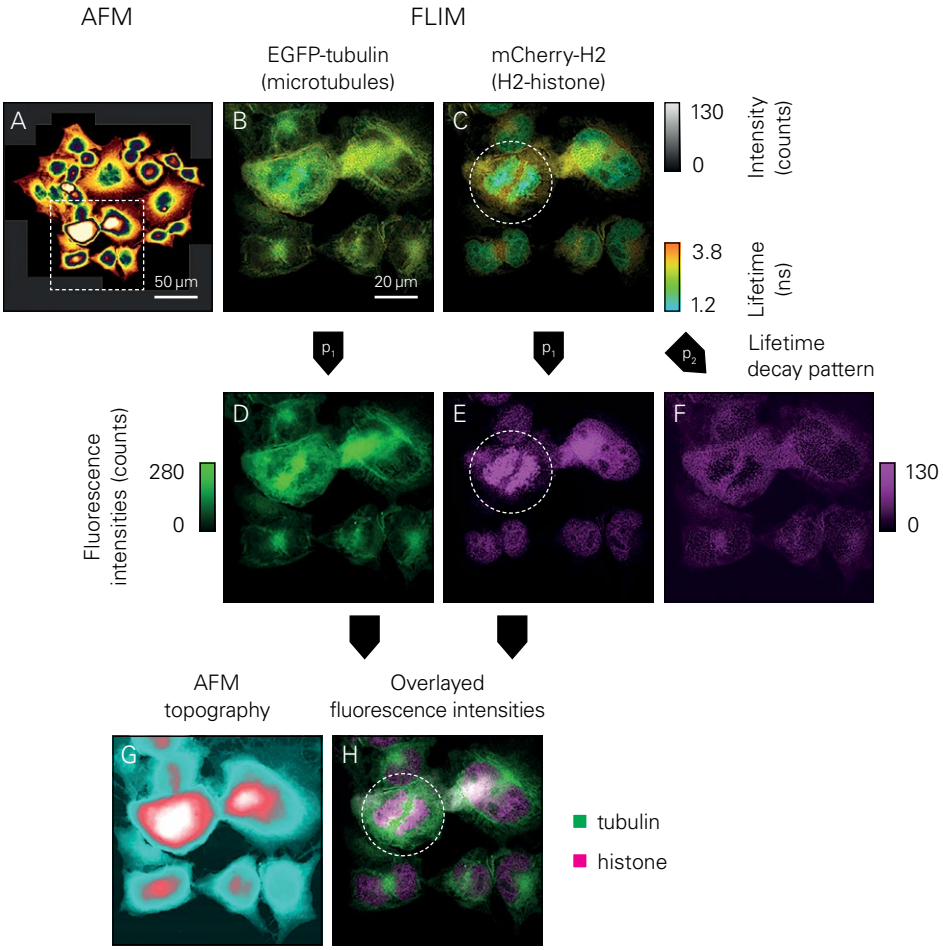

Figure 6

Correlative AFM-FLIM measurements of rehydrated HeLa cells at various stages of the cell cycle. The fluorescent labels used are tubulin-EGFP (for microtubules) and H2B-mCherry (for H2 histones). (A,G) AFM topography channels (QI Advanced mode) were collected with a NanoWizard V BioAFM equipped with a Motorized Precision Stage (Bruker) enabling large-scale area investigations (height range in (G) is 3 µm). The corresponding fluorescence lifetime images from the inset location in (A) for EGFP (microtubules, B) and mCherry (chromatin, C) were recorded with a MicroTime 200 confocal FLIM setup (PicoQuant). A cell in a metaphase cell cycle stage is highlighted. To eliminate the fluorescence background visible in (C), fluorescence intensity images (D-F) for the two identified lifetime patterns are computed. The fluorescence intensity images of pattern P1 for both EGFP and mCherry are then overlaid in (H), providing a clearer view of the metaphase state cellular structures.

One of the advantages of FLIM is its capacity to disentangle fluorescence contributions with varying fluorescence decay patterns, where a pattern can comprise of more than one characteristic decay time τ. While only one decay pattern is present for EGFP (Figure 6D), two distinct decay patterns, corresponding to chromatin-bound histone and predominantly cytoplasmic histone (background), are observed for mCherry (Figures 6E and 6F). By excluding the background and superimposing the fluorescence intensity images of microtubules (pattern P1, green) and chromatin-bound histone (pattern P2, magenta) in Figure 6H, the final reconstructed image can be correlated to the corresponding AFM topography of the same location (Figure 6G).

Investigating Liver Fenestrations with Correlative AFM and STED Microscopy

AFM-STED Microscopy – The Technique

The fundamental principle of STED involves the use of two laser pulses – the first one excites the fluorophores, and the second one de-excites them.[22] The excitation laser scans the sample, while the donut-shaped STED beam, responsible for depletion, extinguishes the fluorophore at the periphery of the focal point, which effectively confines the fluorescence spot (Figure 7A).

This process significantly enhances the resolution beyond the diffraction limit of conventional optical microscopy by an order of magnitude. By selectively depleting the fluorescence around the focal point, STED achieves a much smaller effective point spread function. This allows the visualization of structures at the nanoscale, providing detailed insights into cellular and molecular processes. The combination of AFM with STED microscopy enables correlative imaging, where the topographical information from AFM is complemented by the super-resolution fluorescence data from STED. This integrated approach is particularly useful for studying complex biological samples, where both structural and functional information are crucial.

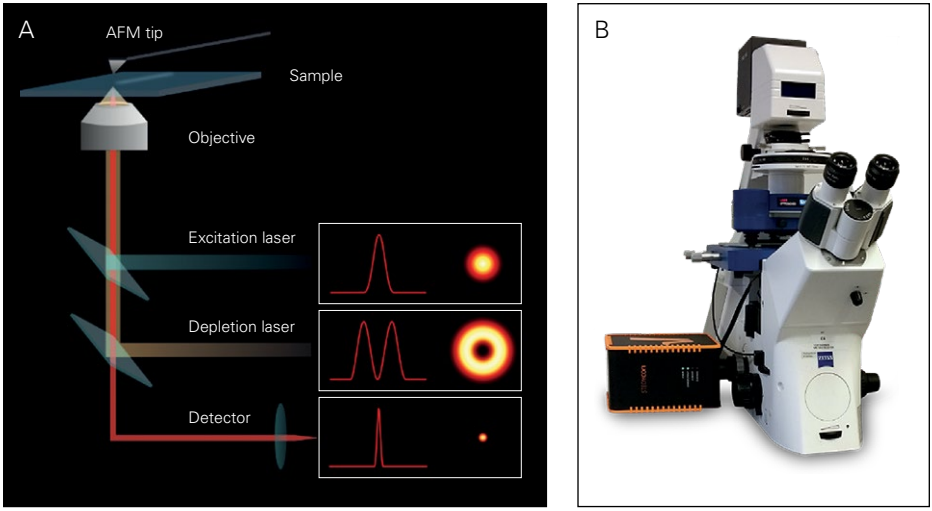

Figure 7

(A) Principle of combined AFM and STED microscopy – the "donut" shape of the encircling depletion (STED) laser confines the spot of effective fluorescence.

(B) NanoWizard family AFM (Bruker) integrated with a compact line STEDYCON (Abberior Instruments) on an AxioObserver (Zeiss).

Investigating Liver Fenestrations using Correlative AFM and STED Microscopy

Liver capillaries, or sinusoids, are structures that are lined by a monolayer of liver sinusoidal endothelial cells (LSECs) that facilitate efficient bidirectional transport through nanometer-sized pores called fenestrations. With an average diameter of 160 nm, the size of these structures is beyond the resolution of traditional optical microscopy.[23] Since their discovery in 1970,[24] the study of their structure was, for the most part, limited to electron microscopy and static images of chemically fixed liver tissues and cells. The advent of AFM and super-resolution microscopy techniques has advanced our current understanding of fenestrations by enabling analysis of hydrated fixed and living LSECs.[25]

These techniques confirmed that fenestrations are dynamic structures that can migrate within the cell, vary in lifespan, and quickly change states, as shown by AFM and STED.[26-28] Optical nanoscopy techniques have further shown that fenestrations are held by an actin-spectrin scaffold.[29,30]

A recent integration of AFM and STED was used to study LSEC fenestrations (Figure 8A-C). Correlative imaging using STED and AFM resulted in precise colocalization of fenestrations in both types of images.[31] The sharper boundaries measured in the AFM images are a direct result of the sharp scanning tips.

In the case of STED, the identification of the fenestration boundaries is limited by the PSF (point spread function) related blurring, which limits its accuracy for identifying pore size to ca. 50 nm. Both techniques provided similar data on the diameter of the fenestrations (with a discrepancy of less than 10 %) as shown in Figure 8D. Pair-wise comparison yielded a strong linear correlation ($r = 0.94$) for both diameter and area (Figures 8F and 8G).

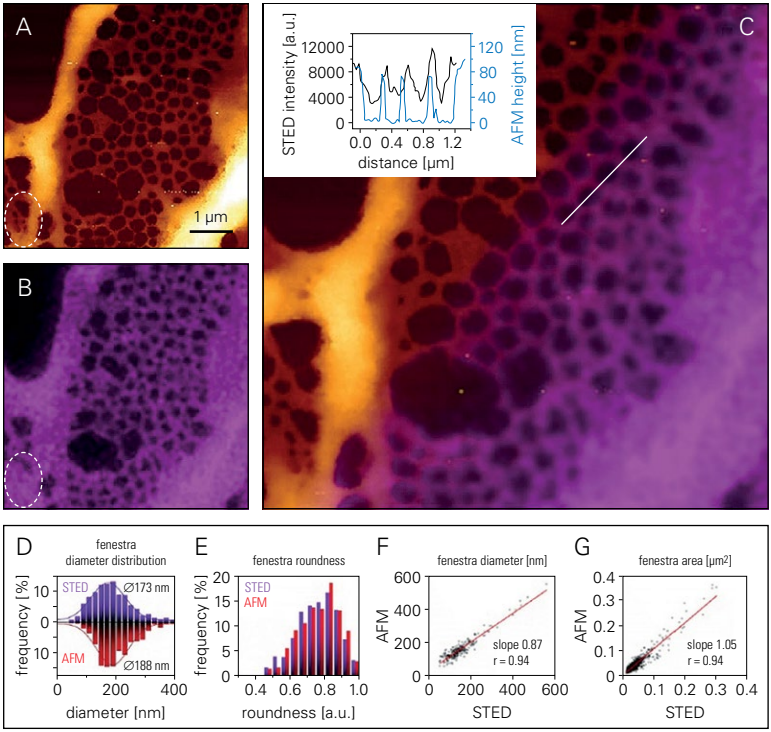

Figure 8

Comparative AFM and STED microscopy measurements of wet, fixed LSECs treated with cytochalasin B.

(A) High-resolution image of a sieve plate in the LSEC periphery measured using AFM.

(B) The corresponding area measured using STED. Fenestrations as small as 50 nm can be distinguished with AFM but not with STED (white dashed circle).

(C) Correlative image of the same area measured using STED and AFM. The inset represents a cross-section of selected fenestrations (white line in (C)). 709 fenestrations were identified in the images collected and analyzed in a one-to-one manner.

(D) Histogram of fenestration diameter distribution. The black lines represent fitted Gaussian curves from which the mean diameters were calculated at the peak of the distribution (STED 173 nm ± 58 nm, AFM 188 nm ± 54 nm).

(E) Distribution of fenestration roundness measured by STED and AFM.
A comparison of individual fenestration diameters (F) and area (G) indicate uniform and precise measurements of fenestrations using both techniques.

The figure was adapted from[31] under the open access usage policy.

Biological objects are soft materials which, in theory, means that structures can be deformed during AFM measurements while the sample surface is being probed with the AFM cantilever. To assess this, several LSEC samples with differing specimen treatment were compared, namely non-modified (live), and formaldehyde (FA) or glutaraldehyde (GA) fixed cells (Figure 9). While GA fixation allowed the uniform preservation of the fenestration diameter across a wide range of forces, it also led to a ten-fold increase in Young's modulus compared to non-FA-treated cells and a two-fold increase in Young's modulus compared to FA-treated LSECs (Figure 8A). This emphasizes that only mechanical data recorded on living cells truly represents the apparent stiffness of the measured cells.

By measuring the LSECs with quantitative imaging (QI) mode, it was possible to apply reference force reconstruction of the fenestration topography under different loading forces. This so called "force tomography" approach enables the unravelling of the underlying structural hierarchies localized under the cell membrane.[32] Furthermore, this technique allows the investigation of fenestration deformability and the degree of morphological change induced by the AFM tip in the fenestration diameter. Increasing force revealed the stiffer actin fiber scaffold, which remained undeformed, while softer parts near the fenestra center were displaced, which corroborates with previous studies.[26]

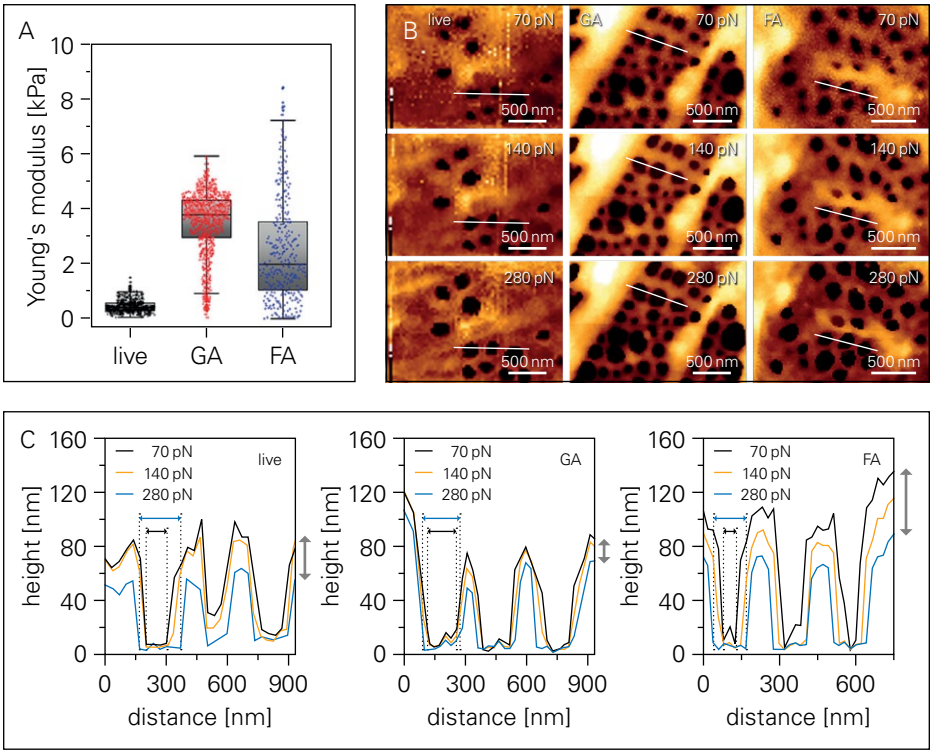

Figure 9

Mechanical properties of fenestrations in living vs. fixed LSECs.

(A) The apparent Young's modulus of cells (n = 15 for each group, 64 curves per cell) was obtained for a colloidal cantilever for a load force of 200 pN.

(B) Images of selected sieve plates measured using QI Mode reconstructed for a load force of 70 pN, 140 pN, and 280 pN.

(C) The tip-induced enlargement of fenestrations presented as a cross-section of selected fenestrations collected for the same area of the images and reconstructed for different load forces. Grey double-headed arrows indicate the tip-induced squeezing of the membrane surrounding fenestrations in the z-axis. Black and blue arrows indicate the boundaries of fenestration obtained at 70 and 280 pN, respectively.

The figure was adapted from[31] under the open access usage policy.

Outlook and Future Trends

The integration of AFM with advanced optical microscopy, as demonstrated by the NanoWizard family of AFMs in this ebook, is paving the way for novel and innovative correlative microscopy research. These integrations allow a comprehensive analysis of biological samples, from the cellular level to tissues and even entire organs in smaller animal models.

The future of this field promises exciting advancements, particularly in live cell imaging, facilitated further by the use of novel advanced super-resolution techniques, such as RESOLFT microscopy (reversible saturable optical fluorescence transition) based on reversibly switchable fluorescent proteins. Another novel technique is MINFLUX microscopy (minimal photon fluxes) that combines the concept of single-molecule localization (used in PALM/STORM) with the structured illumination approach used in STED microscopy. Here the fluorophores in a sample are separated by activating and deactivating them individually per diffraction region. These techniques minimize the exposure of samples to energy and reduce acquisition times considerably.

The simultaneous use of AFM and SIM is another promising technique for the correlative imaging of cells[33] and is an excellent alternative to certain super-resolution techniques where high-powered lasers can lead to a deterioration of the sample being investigated. The incorporation of FLIM could provide additional insights into dynamic processes in cells by measuring fluorescence lifetimes, allowing researchers, for example, to track the distribution of membrane proteins with optical microscopy and their positions on the cell using AFM, thus taking correlative microscopy to unprecedented levels of detail and understanding.

These advancements are expected to revolutionize our understanding of biological systems and create new avenues for research and therapeutic approaches.

Acknowledgements

The authors would like to thank Tanja Neumann for her assistance with the AFM-STED measurements. We are also grateful to Maria Loidolt-Krüger (PicoQuant) for providing the HeLa samples, technical support during the FLIM measurements, and reviewing the ebook.

Authors

[1] Bartłomiej Zapotoczny
Department of Biophysical Microstructures, Institute of Nuclear Physics, Polish Academy of Sciences, Kraków, Poland

[2] Thomas Fuhs, Joerg Barner, Dimitar R. Stamov, Thomas Henze
Bruker BioAFM, Berlin, Germany

References

[1] Abbe E (1873) Beiträge zur Theorie des Mikroskops und der mikroskopischen Wahrnehmung, Arch Für Mikrosk Anat 9 (1), 413-468, https://doi.org/10.1007/BF02956173

[2] Binnig G, Quate CF, Gerber Ch (1986) Atomic Force Microscope, Phys Rev Lett 56 (9), 930-933, https://doi.org/10.1103/PhysRevLett.56.930

[3] Smith C (2012) Two microscopes are better than one, Nature 492 (7428), 293-297, https://doi.org/10.1038/492293a

[4] Valli J, Garcia-Burgos A, Rooney LM, Vale De Melo E Oliveira B, Duncan RR, Rickman C (2021) Seeing beyond the limit: A guide to choosing the right super-resolution microscopy technique, J Biol Chem 297 (1), 100791, https://doi.org/10.1016/j.jbc.2021.100791

[5] Gómez-Varela AI, Stamov DR, Miranda A, Alves R, Barata-Antunes C, Dambournet D, Drubin DG, Paiva S, De Beule PAA (2020) Simultaneous co-localized super-resolution fluorescence microscopy and atomic force microscopy: combined SIM and AFM platform for the life sciences, Sci Rep 10 (1), 1122, https://doi.org/10.1038/s41598-020-57885-z

[6] Monserrate A, Casado S, Flors C (2014) Correlative Atomic Force Microscopy and Localization-Based Super-Resolution Microscopy: Revealing Labelling and Image Reconstruction Artefacts, ChemPhysChem 15 (4), 647-650, https://doi.org/10.1002/cphc.201300853

[7] Hargreaves RB, Rozario AM, McCoy TM, Meaney SP, Funston AM, Tabor RF, Whelan DR, Bell TDM (2022) Optimising correlative super resolution and atomic force microscopies for investigating the cellular cytoskeleton, Methods Appl Fluoresc 10 (4), 045005, https://doi.org/10.1088/2050-6120/ac8526

[8] Curry N, Ghézali G, Kaminski Schierle GS, Rouach N, Kaminski CF (2017) Correlative STED and Atomic Force Microscopy on Live Astrocytes Reveals Plasticity of Cytoskeletal Structure and Membrane Physical Properties during Polarized Migration, Front Cell Neurosci 11 104, https://doi.org/10.3389/fncel.2017.00104

[9] Owen RJ, Heyes CD, Knebel D, Röcker C, Nienhaus GU (2006) An integrated instrumental setup for the combination of atomic force microscopy with optical spectroscopy, Biopolymers 82 (4), 410-414, https://doi.org/10.1002/bip.20414

[10] Höppener C, Elter JK, Schacher FH, Deckert V (2023) Inside Block Copolymer Micelles – Tracing Interfacial Influences on Crosslinking Efficiency in Nanoscale Confined Spaces, Small 19 (20), 2206451, https://doi.org/10.1002/smll.202206451

[11] Pfitzner E, Heberle J (2020) Infrared Scattering-Type Scanning Near-Field Optical Microscopy in Water, ChemRxiv (preprint), https://doi.org/10.26434/chemrxiv.12279551.v1

[12] Meredith SA, Yoneda T, Hancock AM, Connell SD, Evans SD, Morigaki K, Adams PG (2021) Model Lipid Membranes Assembled from Natural Plant Thylakoids into 2D Microarray Patterns as a Platform to Assess the Organization and Photophysics of Light-Harvesting Proteins, Small 17 (14), 2006608, https://doi.org/10.1002/smll.202006608

[13] Schulz O, Zhao Z, Ward A, Koenig M, Koberling F, Liu Y, Enderlein J, Yan H, Ros R (2013) Tip induced fluorescence quenching for nanometer optical and topographical resolution, Opt Nanoscopy 2 (1), 1, https://doi.org/10.1186/2192-2853-2-1

[14] Fernandes TFD, Saavedra-Villanueva O, Margeat E, Milhiet P-E, Costa L (2020) Synchronous, Crosstalk-free Correlative AFM and Confocal Microscopies/Spectroscopies, Sci Rep 10 (1), 7098, https://doi.org/10.1038/s41598-020-62529-3

[15] Thompson AJ, Pillai EK, Dimov IB, Foster SK, Holt CE, Franze K (2019) Rapid changes in tissue mechanics regulate cell behaviour in the developing embryonic brain, eLife 8 e39356, https://doi.org/10.7554/eLife.39356

[16] Morr AS, Nowicki M, Bertalan G, Vieira Silva R, Infante Duarte C, Koch SP, Boehm-Sturm P, Krügel U, Braun J, Steiner B, Käs JA, Fuhs T, Sack I (2022) Mechanical properties of murine hippocampal subregions investigated by atomic force microscopy and in vivo magnetic resonance elastography, Sci Rep 12 (1), 16723, https://doi.org/10.1038/s41598-022-21105-7

[17] Mages B, Fuhs T, Aleithe S, Blietz A, Hobusch C, Härtig W, Schob S, Krueger M, Michalski D (2021) The Cytoskeletal Elements MAP2 and NF-L Show Substantial Alterations in Different Stroke Models While Elevated Serum Levels Highlight Especially MAP2 as a Sensitive Biomarker in Stroke Patients, Mol Neurobiol 58 (8), 4051-4069, https://doi.org/10.1007/s12035-021-02372-3

[18] Bugiel I, König K, Wabnitz H (1989) Investigation of Cells by Fluorescence Laser Scanning Microscopy with Subnanosecond Time Resolution, Lasers Life Sci 3 (1), 47-53.

[19] Lakowicz JR, Szmacinski H, Nowaczyk K, Berndt KW, Johnson M (1992) Fluorescence lifetime imaging, Anal Biochem 202 (2), 316-330, https://doi.org/10.1016/0003-2697(92)90112-K

[20] Lakowicz JR, Szmacinski H, Nowaczyk K, Johnson ML (1992) Fluorescence lifetime imaging of free and protein-bound NADH., Proc Natl Acad Sci 89 (4), 1271-1275, https://doi.org/10.1073/pnas.89.4.1271

[21] Oida T, Sako Y, Kusumi A (1993) Fluorescence lifetime imaging microscopy (flimscopy). Methodology development and application to studies of endosome fusion in single cells, Biophys J 64 (3), 676-685, https://doi.org/10.1016/S0006-3495(93)81427-9

[22] Hell SW, Wichmann J (1994) Breaking the diffraction resolution limit by stimulated emission: stimulated-emission-depletion fluorescence microscopy, Opt Lett 19 (11), 780, https://doi.org/10.1364/OL.19.000780

[23] Szafranska K, Kruse LD, Holte CF, McCourt P, Zapotoczny B (2021) The wHole Story About Fenestrations in LSEC, Front Physiol 12 735573, https://doi.org/10.3389/fphys.2021.735573

[24] Wisse E (1970) An electron microscopic study of the fenestrated endothelial lining of rat liver sinusoids, J Ultrastruct Res 31 (1-2), 125-150, https://doi.org/10.1016/S0022-5320(70)90150-4

[25] Shami GJ, Zapotoczny B, Wisse E, Braet F (2024) Microscopic imaging of hepatic sinusoidal cells: Fifty years in the making. In: Sinusoidal Cells in Liver Diseases. Elsevier, pp 89-110, https://doi.org/10.1016/B978-0-323-95262-0.00005-X

[26] Zapotoczny B, Szafranska K, Owczarczyk K, Kus E, Chlopicki S, Szymonski M (2017) Atomic Force Microscopy Reveals the Dynamic Morphology of Fenestrations in Live Liver Sinusoidal Endothelial Cells, Sci Rep 7 (1), 7994, https://doi.org/10.1038/s41598-017-08555-0

[27] Di Martino J, Mascalchi P, Legros P, Lacomme S, Gontier E, Bioulac-Sage P, Balabaud C, Moreau V, Saltel F (2019) Actin Depolymerization in Dedifferentiated Liver Sinusoidal Endothelial Cells Promotes Fenestrae Re-Formation, Hepatol Commun 3 (2), 213-219, https://doi.org/10.1002/hep4.1301

[28] Zapotoczny B, Szafranska K, Kus E, Braet F, Wisse E, Chlopicki S, Szymonski M (2019) Tracking Fenestrae Dynamics in Live Murine Liver Sinusoidal Endothelial Cells, Hepatology 69 (2), 876-888, https://doi.org/10.1002/hep.30232

[29] Mönkemöller V, Øie C, Hübner W, Huser T, McCourt P (2015) Multimodal super-resolution optical microscopy visualizes the close connection between membrane and the cytoskeleton in liver sinusoidal endothelial cell fenestrations, Sci Rep 5 (1), 16279, https://doi.org/10.1038/srep16279

[30] Zapotoczny B, Braet F, Kus E, Ginda-Mäkelä K, Klejevskaja B, Campagna R, Chlopicki S, Szymonski M (2019) Actin-spectrin scaffold supports open fenestrae in liver sinusoidal endothelial cells, Traffic 20 (12), 932-942, https://doi.org/10.1111/tra.12700

[31] Szafranska K, Neuman T, Baster Z, Rajfur Z, Szelest O, Holte C, Kubisiak A, Kus E, Wolfson DL, Chlopicki S, Ahluwalia BS, Lekka M, Szymonski M, McCourt P, Zapotoczny B (2022) From fixed-dried to wet-fixed to live – comparative super-resolution microscopy of liver sinusoidal endothelial cell fenestrations, Nanophotonics 11 (10), 2253-2270, https://doi.org/10.1515/nanoph-2021-0818

[32] Czyzynska-Cichon I, Kotlinowski J, Blacharczyk O, Giergiel M, Szymanowski K, Metwally K, Wojnar-Lason K, Dobosz E, Koziel J, Lekka M, Chlopicki S, Zapotoczny B (2024) Early and late phases of liver sinusoidal endothelial cell (LSEC) defenestration in mouse model of systemic inflammation. Cell Mol Biol Lett (accepted).

[33] Gómez-Varela AI, Stamov DR, Miranda A, Alves R, Barata-Antunes C, Dambournet D, Drubin DG, Paiva S, De Beule PAA (2020) Simultaneous co-localized super-resolution fluorescence microscopy and atomic force microscopy: combined SIM and AFM platform for the life sciences, Sci Rep 10 (1), 1122, https://doi.org/10.1038/s41598-020-57885-z

Further Resources

Bruker's AFM Solutions for Life Sciences Research:
https://www.bruker.com/bioafm

BioAFM Accessories:
https://www.bruker.com/en/products-and-solutions/microscopes/bioafm/bioafm-accessories.html

Suscribe to our Journal Club to keep up to date on the latest in BioAFM Research:
https://www.bruker.com/en/products-and-solutions/microscopes/bioafm/bioafm-journal-club.html

JPK BioAFM Business
Nano Surfaces and Metrology Division
Bruker Nano GmbH

Am Studio 2D · 12489 Berlin, Germany
tel.: +49 30 670990 7500 · fax: +49 30 670990 30

www.bruker.com/bioafm

Contact us!